US.6
A32A1

research review

OFFICE of AEROSPACE RESEARCH

OAR: The Research Agency
of The United States Air Force

VOLUME V NUMBER 9 NOVEMBER 1966

THE EFFECT OF AERODYNAMIC CONTROL SURFACES ON HIGH-SPEED VEHICLES

MAJOR JOHN P. THOMAS, Hypersonic Research Laboratory, ARL

A study of the effect of aerodynamic control surfaces on hypersonic vehicles has been in progress for some time at ARL. The investigation encompasses various shaped fins on a blunt flat plate. Figure 1 shows the experimental test model. The fins as well as the blunt flat plate were tested at different angles. Chordwise pressure distributions were recorded on the surface of the blunt flat plate for the various configurations. An analytical approach to the same problem was conceived, and its results were compared to the results of the experimental work.

The need for this type of study becomes apparent when one realizes that the next generation of re-entry vehicles, HL-10, SV-5, and scramjet, are lifting configurations with aerodynamic control surfaces for guidance in the earth's atmosphere. Figure 2 gives an artist's conception of such a vehicle. In addition, before too long, the USAF will be flying aircraft at hypersonic speeds. With these two important advancements in flying vehicles just over the horizon, a study of the flow patterns, pressure distributions, and heating on the vehicles caused by the movement of control surfaces assumes great significance for the aerospace engineers and scientists.

Problems are encountered in the hypersonic speed range which have not affected vehicles flying at slower speeds. Some of the minor problems which are present at lower speeds become magnified as the vehicle increases its flight velocity. One of the problems which becomes more pronounced at hypersonic speeds is the separation of the flow about the vehicle due to adverse pressure gradients caused by shocks in the flow field. If the position and magnitude of the adverse pressure gradient may be estimated, then the effect on the over-all vehicle performance can be approximated. The present study was undertaken to examine the possibility of predicting the pressure gradients caused by control surfaces as well as to gain experimental data needed by the designer.

The experimental work was accomplished in one of ARL's 4-inch hypersonic wind tunnels. Four different fins were tested on a blunt flat plate. The fin yaw angle and plate angle of attack were varied during the testing. Pressures at the surface of the flat plate were mapped for some distance on either side of the fin and from the leading to the trailing

edge of the plate. Figure 1 gives a view of the blunt plate with a blunt unswept fin installed. In Figure 3, the circles are the measured pressures of the plate shown as a ratio with the free-stream pressure versus the distance aft of the leading edge of the plate nondimensionalized by the thickness of the plate. (Figure 3 represents data for a wing attack angle of 0^{o}, fin yaw angle of 0^{o}, and a spanwise distance on the plate of 0.1 inch from the fin centerline.)

For the analytical approach to the prediction of the pressure distribution on the blunt plate, it is first necessary to establish an inviscid solution which represents the flow if no boundary layer existed on the plate. The results of the inviscid estimation are shown by the dotted curve of Figure 3. The method is given in Ref. 3. Note the discontinuity in the pressure distribution at $x/d = 10.2$. For the viscid case, the discontinuity is not possible because the adverse pressure gradient is carried upstream through the subsonic portion of the boundary layer which exists for viscid flow. An adverse pressure gradient, if strong enough, will cause the boundary layer to separate from the surface of the plate. Downstream of the separation point the boundary layer has two alternatives, depending on the flow conditions. First, the boundary layer may remain separated downstream of the original separation point, or second, the layer may reattach to the plate downstream of the separation point. In the case shown in Figure 3, the experimental pressures indicate a separation and reattachment of the flow. To approximate analytically the experimental flow conditions, a method by Lees and Reeves (Ref. 1), with simplifying assump-

research review
OFFICE OF AEROSPACE RESEARCH

OAR RESEARCH REVIEW is published monthly by the Office of Scientific and Technical Information (RRYC), Hq Office of Aerospace Research, USAF, 1400 Wilson Boulevard, Arlington, Va. 22209. The objective of this publication is to make a positive contribution to the exchange of information concerning Air Force conducted and sponsored research activities.

JACOB SEIDEN
Editor

THE EFFECT OF AERODYNAMIC CONTROL SURFACES ON HIGH-SPEED VEHICLES
Major John P. Thomas 1

ELECTRON ACCEPTORS
Dr. Tapan K. Mukherjee 4

NUMERICAL INTEGRATION OF THE NAVIER–STOKES EQUATION
Lt Col Barnett R. Agins 6

THE MÖSSBAUER EFFECT IN EXTERNAL MAGNETIC FIELDS
Max Swerdlow 7

A STEP FORWARD IN CERAMIC STORAGE–HEATER DESIGN
Norman E. Scaggs 14

TURBULENT HEAT TRANSFER IN AN INSULATED PIPE
J. W. Goresh 18

LIGHT–SCATTERING HOMODYNE SPECTROSCOPY
Electronics Division, AFOSR 21

DOG SILHOUETTES AND OTHER ARBITRARY SHAPES BY COMPUTER
Data Sciences Laboratory, AFCRL 23

DISTRIBUTION OF THIS DOCUMENT IS UNLIMITED

For sale by the Superintendent of Documents, U.S. Government Printing Office Washington, D.C. 20402 - $2.75 per year domestic, 75 cents additional for foreign mailing, 25 cents per single copy and 15 cents per Annual Index. Back issues will not be furnished.

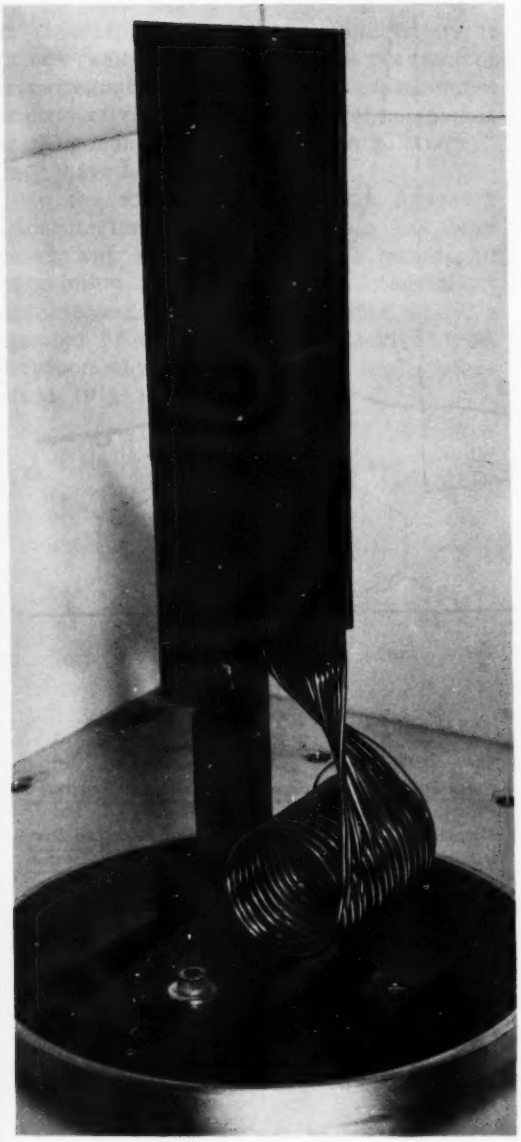

Figure 1.

Photograph of Wing-Fin Wind-Tunnel Model.

tions by Hankey and Cross (Ref. 2), was used. The complete method of establishing the analytical flow field on the plate about the fin is shown for blunt leading-edge fins with and without sweep in Ref. 3. The procedure consists of a strip method which allows the two-dimensional Lees and Reeves approach to be extended to the three-dimensional problem of the flow about the base of the fin. Results of the analytical approach to the problem are shown by the continuous curve in Figure 3. The symbol x gives the analytical separation point, while Δ shows the reattachment location. In the analytical method it is possible to predict whether separation will occur or not.

With the knowledge gained from this study, it now becomes possible to predict the pressure distribution on a vehicle flying hypersonically, and to use the pressure distribution to approximate the heat-transfer distribution. Through basic-research efforts like this, the aerospace designer will have better means available to him on which to base his design concepts, now and in the future, for USAF flight vehicles.

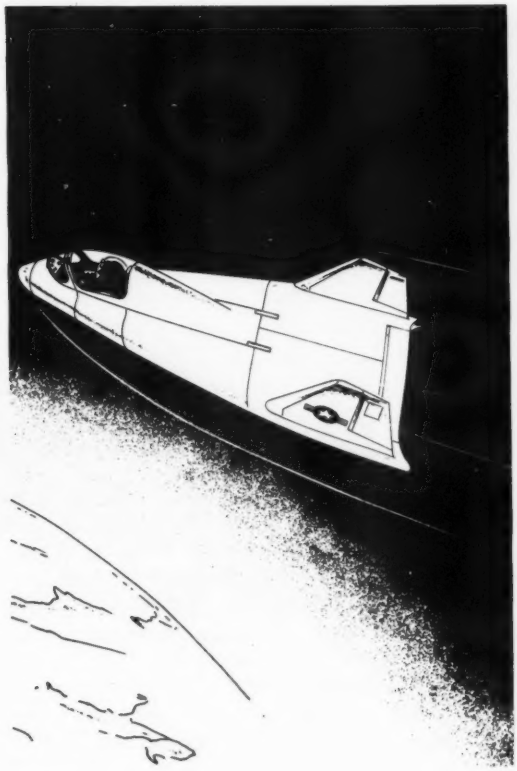

Figure 2.

Artist's Concept of Lifting Hypersonic Vehicle.

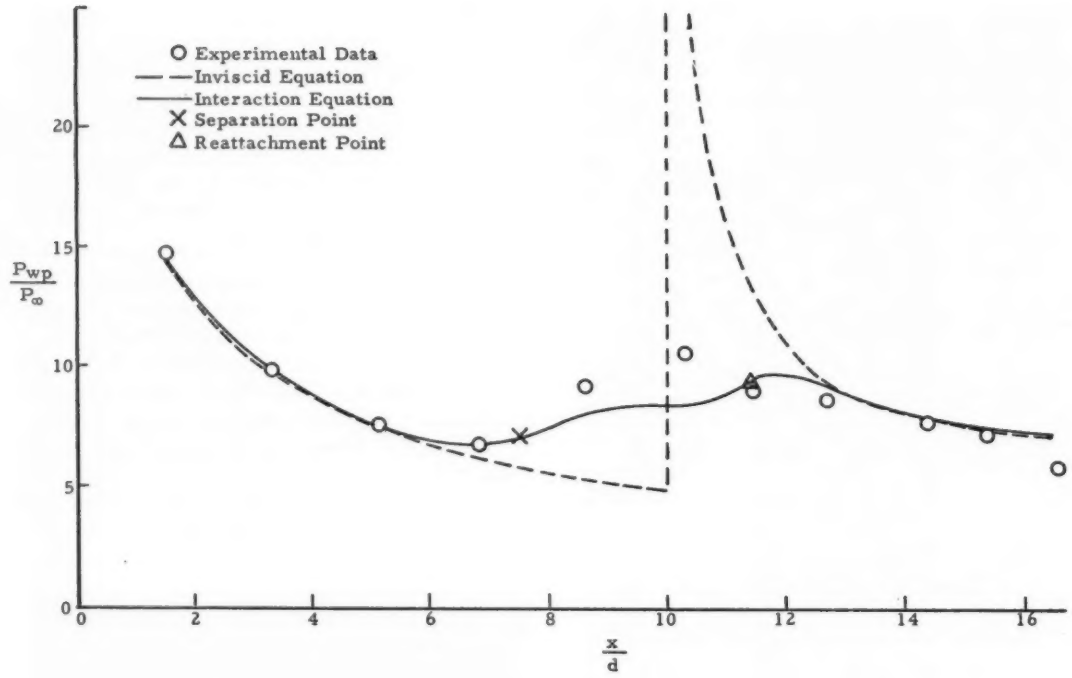

Figure 3. Flat Plate Pressure $\Lambda = 0°, \alpha = 0°, \delta = 0°, y = 0.1$ *inch.*

REFERENCES

(1) Lees, L. and B. L. Reeves, "Supersonic Separated and Reattaching Laminar Flows. I. General Theory and Application to Adiabatic Boundary-Layer/Shock-Wave Interactions," AIAA Journal, 2, 1964.

(2) Hankey, W. L. and E. J. Cross, Approximate Closed Form Solutions for Supersonic Laminar Separated Flows, to be published.

(3) Thomas, J. P., Investigation of the Pressure Distribution on a Blunt-Fin Blunt-Plate Combination at a Mach Number of 11.26, Ph.D. Dissertation, The Ohio State University, 1966. (In publication as an ARL report.) ★

ELECTRON ACCEPTORS

DR. TAPAN K. MUKHERJEE, Space Physics Laboratory, AFCRL

In recent years, research on the phenomenological and electronic application aspects of organic charge-transfer complexes has greatly intensified. These complexes are formed when an acceptor molecule reacts with an appropriate donor molecule. Compounds with electronegative substituents function as acceptors, whereas aromatic hydrocarbons, amines, etc., with available π-electron clouds or lone pairs of electrons constitute the donors. The stability of charge-transfer complexes depends largely on the electron affinity of the acceptors and the ionization potential of the donors. When an acceptor of high electron affinity reacts with a donor of sufficiently low ionization potential, one electron may be completely transferred from the donor to the acceptor, resulting in the formation of paramagnetic ion-radicals. Electrical conductivities of solid charge-transfer complexes and ion-radicals have become an exceedingly interesting property, especially for their potential semiconductor applications. Although organic molecules are,

in general, poor conductors of electricity, it is now well established that the presence of free-radical species causes an enhancement of conductivity. Thus, ion-radical complexes in the conductivity range, 10^{1} to 10^{-1} ohm $^{-1}$ cm^{-1} have been synthesized.

At the Air Force Cambridge Research Laboratories, a broad program has been under way aimed at deriving a meaningful correlation between electronic conductivity and molecular structure. In this study, a mumber of electron acceptors derived from dicyanomethylene fluorene have been synthesized. (Fig. 1)

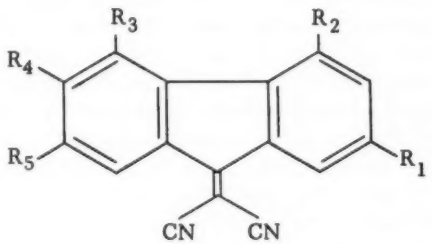

(a) $R_1, R_2, = NO_2$; $R_3, R_4, R_5 = H$

(b) $R_1, R_3 = NO_2$; $R_2, R_4, R_5 = H$

(c) $R_1, R_4, = NO_2$; $R_2, R_3, R_5 = H$

(d) $R_1, R_5, = NO_2$; $R_2, R_3, R_4 = H$

(e) $R_1, R_2, R_5 = NO_2$; $R_3, R_4 = H$

(f) $R_1, R_2, R_3, R_5 = NO_2$; $R_4 = H$

Figure 1

Electron affinities, relative to 2,4,7-trinitrofluorenone, were determined from spectral studies of the charge-transfer complexes of these acceptors with a number of aromatic hydrocarbons as donors (1). The electron affinities of the dinitro-isomers vary according to the orientation of the substituents. Increasing the number of nitro groups on the basic acceptor structure causes marked enhancement of the electron affinity. Thus, the 2,4,7-trinitro derivative (e) and the 2,4,5,7-tetranitro derivative (f) are found to be strong acceptors (2) (3). These compounds form highly colored, insoluble complexes with polycyclic aromatic hydrocarbons and amines, and are useful as complexing reagents in analytical chemistry. The stability of some of these complexes is of such high order that they can be purified by recrystallization. These acceptors do not undergo displacement reactions with amines or Diels-Alder type reactions with aromatic hydrocarbons, thus showing distinct advantages over tetracyanoethylene, a more powerful acceptor. Dicyanomethylene 2,4,7-trinitrofluorene (e) has been marketed by Eastman Chemicals as a complexing reagent.

Stable anion radical salts can be conveniently prepared from the tri- and tetranitro derivatives and suitable donors. Radical salts with organic cations have also been synthesized by the metathetical reaction between the lithium salts of these compounds and ammonium, arsonium or phosphonium iodides. These salts show typical semiconductor properties, with conductivities in the 10^{-3} to 10^{-9} ohm^{-1} cm^{-1} range.

In another aspect of the current research, it has been found that these electron acceptors show variable photoconductivity. The conductivity of the 2,7-dinitro derivative (d) is enhanced by 4 orders of magnitude when this material is illuminated by a 200-watt lamp from a distance of 7 cm. Contrary to the general experience, the photocurrent maximum lies considerably beyond the absorption maximum of the compound. This is the first reported case of high photoconduction efficiency encountered in organic electron acceptors. Its implication for the conduction phenomena in molecular crystals is being actively investigated. ★

REFERENCES

(1) Briegleb, G., Angew. Chem., 76, 326, 1964.

(2) Mukherjee, T. K. and L. A. Levasseur, J. Org. Chem., 30, 644, 1965.

(3) Mukherjee, T. K. and A. Golubovic, Abs. 149th Meeting of Am. Chem. Soc., April 1965, p. 53P.

numerical integration of the Navier-Stokes equation

LT COL BARNETT R. AGINS
Directorate of Mathematical Sciences, AFOSR

The motion of a disturbed viscous fluid is important in many areas, such as flow about aerospace vehicles in flight and flow in a tube or channel. The general representation of this phenomenon is the Navier-Stokes equation, which is a nonlinear, elliptic, partial differential equation. A considerable number of results have been obtained by analytic means on estimates and bounds of solutions; however, for detailed results, it is necessary to turn to numerical methods.

Working under a grant from the Applied Mathematics Division, AFOSR, Prof. J. Gillis of the Weizmann Institute of Science has been developing techniques for the numerical solution of this equation. To demonstrate his theory and obtain further insight, the techniques were first applied to the problem of the steady-state, two-dimensional flow of a homogeneous, incompressible viscous fluid in the inlet region of a straight channel. (1) Values of Reynolds number ranging from 0 to 500 were used.

The problem was formulated, using the equations:

$$\mu \frac{\delta \mu}{\delta x} + v \frac{\delta \mu}{\delta y} = -\frac{1}{\rho} \frac{\delta p}{\delta x} + \nu \nabla^2 \mu$$

$$\mu \frac{\delta v}{\delta x} + v \frac{\delta v}{\delta y} = \frac{1}{\rho} \frac{\delta p}{\delta y} + \nu \nabla^2 v$$

$$\frac{\delta \mu}{\delta x} + \frac{\delta v}{\delta y} = 0$$

where μ, v are the components of fluid velocity parallel and perpendicular, respectively, to the walls; p is the fluid pressure; ρ the density and ν the kinematic viscosity, both of which are assumed constant.

The walls of the channel are defined by $y = \pm a$ and the inlet by $X = 0$. The boundary conditions are:

$$\mu(0,y) = \mu_0$$
$$v(0,y) = 0$$
$$\mu(x,\pm a) = v(x,\pm a) = 0 \qquad x > 0.$$

It was assumed that the velocity profile at infinity was parabolic; i.e., as $x \to \infty$, $v \to 0$ and

$$\mu \to \frac{3\mu_0}{2a^2}(a^2 - y^2).$$

Integration was performed by establishing finite difference equations with boundary conditions and using a relaxation system.

The results were quite interesting, particularly with respect to the velocity profile. All approximate boundary-layer treatments of this problem assume a convex velocity profile with a maximum on the axis. For small values of x and finite Reynolds number, this is not true. For small x, the parallel component of velocity μ has a local minimum on the axis $y = 0$ and two symmetrically placed maxima on either side of the axis.

A physical argument can be made as follows:

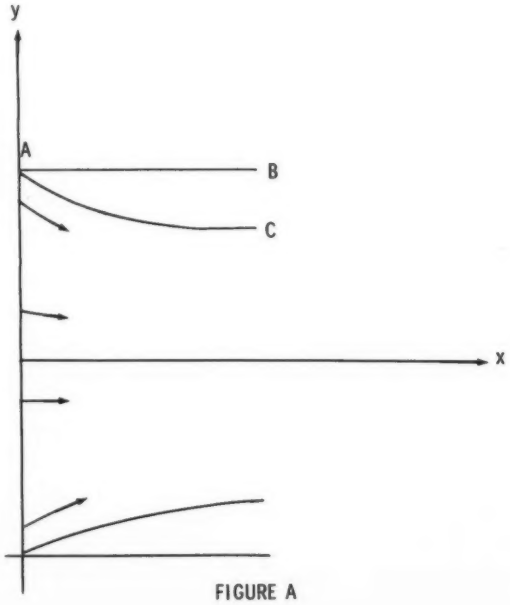

FIGURE A

Consider the straight boundary, AB, and the outer limit, AC, of the boundary layer. The thickness of the boundary layer increases as x^{α} where $\alpha < 1$. It follows that, in the vicinity of A, the rate of increase of thickness as a function of x is very large. This would cause a crowding of streamlines in the core, and a consequent increase of μ in the vicinity of AC. Presumably, it is necessary to travel some distance along the channel before the acceleration of the core, due to the slowing down at the walls, reaches the axis. (This phenomenon has been reported as actually observed in a fluid channel.) The graph of Fig. B shows the velocity profile for the case R = 20; but this situation holds for all values of R investigated with no qualitative change.

Numerical results have been tabulated, including the distance to the parabolic regime.

The numerical technique was applied to the case of an incompressible conducting fluid in the inlet region of a straight channel in the presence of a transverse magnetic field. (2) Similar results were obtained and tabulated.

These results have been applied by Air Force contractors to verify approximate analytic solutions to the problem, and to determine the length of the unstable region for the design of fluid amplifiers. In both cases, the availability of the tabulated results has saved, in computer time, many times the cost of the investigation. ★

REFERENCES

(1) Gillis, J. and A. Brandt, "The Numerical Integration of the Equations of Motion of a Viscous Fluid," AFOSR 65-0629, October 1964.

(2) Brandt, A. and J. Gillis, "Magnetohydrodynamic Flow in the Inlet Region of a Straight Channel," to be published.

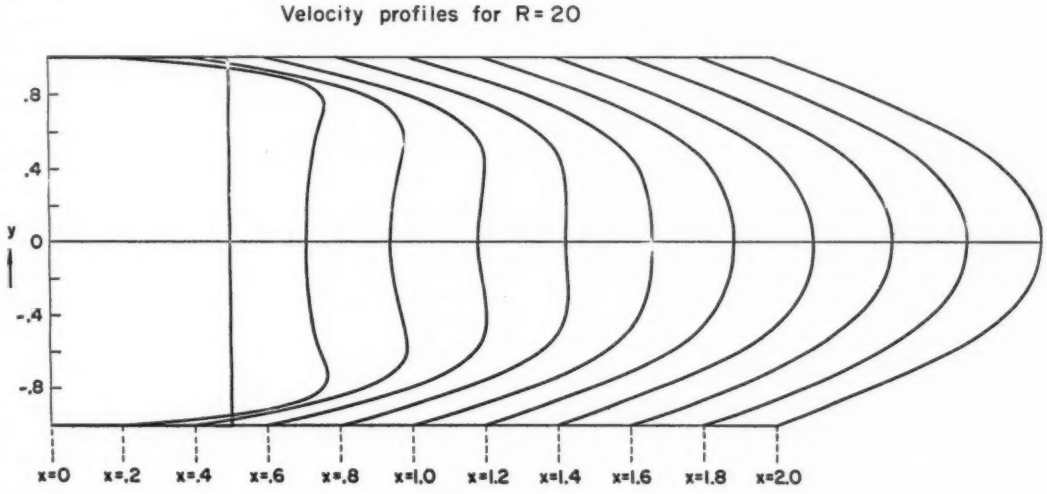

FIGURE B

THE MÖSSBAUER EFFECT IN EXTERNAL MAGNETIC FIELDS

MAX SWERDLOW, Directorate of Physical Sciences, AFOSR

The application of the Mössbauer effect to solid-state physics is now firmly established as a major new tool for probing the structure of matter. When combined with strong magnetic fields its versatility is greatly extended, enabling studies of hyperfine phenomena in materials not possible in zero magnetic field. Such materials include paramagnetic metals, salts, and alloys.

By far, the largest application of the Mössbauer effect has been to the study of hyperfine interactions in magnetic materials.

This is a rewarding pursuit because the experimental determination of hyperfine interactions, particularly magnetic hyperfine interactions, gives a measure of precisely those electronic quantities which are also intimately related to the causes of magnetism. The use of high external magnetic fields often plays an important role in these experiments. For the study of paramagnetic metals, alloys, and salts, high magnetic fields are, in fact, indispensable. Although nuclear magnetic resonance may be used to obtain some of the same information as obtained with the Mössbauer effect, nuclear magnetic resonance requires the use of rf fields, which limits its applicability in superconductors and in many metal single crystals. For these reasons, and others, Mössbauer measurements will continue to be a useful tool for solid-state studies. The mechanism of the Mössbauer effect has been discussed previously in these pages*, and will not be repeated here.

Because iron is one of the transition elements having an unfilled third electronic shell, it exhibits a strong tendency toward magnetic behavior: ferromagnetic in the case of metallic iron, ferrimagnetic in a large number of insulating compounds, antiferromagnetic in a number of substances including α-Fe_2O_3 below 250°K and γ-Fe_2O_3, and paramagnetic in certain dilute alloys and crystals. Since Fe^{57} (parent isotope Co^{57}) is generally considered to be the best isotope in which to observe the Mössbauer effect, it is a natural choice for the Mössbauer study of magnetic phenomena.

If a monochromatic source of the 14.4 keV gamma radiation from Co^{57} (Fe^{57}) is used to irradiate an absorber containing Fe^{57}, an absorption spectrum may be obtained by velocity modulation of the source with respect to the absorber (i.e., Doppler-shifting the energy between the two). In general, three distinct pieces of hyperfine-structure information may be obtained from such a spectrum: (1) the density of s-electrons at the Fe^{57} nucleus (isomer shift); (2) the gradient of the electric field at the nucleus due to the surrounding charge configuration (quadrupole splitting); and (3) the magnitude of the magnetic field interacting with the magnetic moment of the nucleus. The detailed interpretation of all of these effects, singly or in combination, is rather complicated and will not be discussed here. The three simplest possible cases are illustrated in Fig. 1 where (a) shows the effect of an isomer shift as a displacement of the center of the resonance line from zero velocity; (b) shows a quadrupole splitting which results in two resonance lines separated by the energy of the electric quadrupole interaction; and (c) shows the six-line hyperfine pattern which arises from a single magnetic field acting on the Fe^{57} nucleus. In general, all three interactions may coexist; furthermore, some essential characteristics of the spectra depend upon the relative orientations among the electric-field gradient, hyperfine magnetic field vector, and γ-ray propagation direction. In order to simplify our discussion of magnetic phenomena, we shall confine ourselves to a consideration of the magnetic hyperfine spectrum only and disregard the isomer shift and quadrupole interactions; this is permissible because, in the systems we shall discuss in detail, the quadrupole hyperfine interaction is small and does not appreciably distort the spectrum which is due to a magnetic hyperfine interaction only, while the isomer shift simply shifts the center of the spectrum with respect to zero velocity.

In magnetically ordered systems, there is a magnetic hyperfine field at the Fe^{57} nucleus due to the magnetic polarization of some of the electrons which interact with the dipole moment of the nucleus. This gives rise to a spectrum similar to that shown in Fig. 1 (c), where the magnitude of the hyperfine field (approx. 330 kOe in metallic iron and 500 kOe in most magnetically ordered Fe^{3+} compounds) is proportional to the splitting between symmetric pairs of lines; thus the lines are sharp in the presence of a unique hyperfine field. The intensities of the lines marked β are proportional to $\frac{4 \sin^2 \theta}{3(1 + \cos^2 \theta)}$ with respect to the outer pair of lines, where θ is the angle between the effective magnetic

*See OAR Research Review, Nov. 1965, "Surface Studies and the Mössbauer Effect."

hyperfine field vector and the γ-ray propagation direction. Thus, the relative intensity of these (middle) lines tells us the direction of the hyperfine field. For example, if the hyperfine field H_n is parallel to the γ-ray direction z, the middle lines vanish as shown in Fig. 2(a); if H_n is perpendicular to z, the six lines have relative intensities 3:4:1:1:4:3,

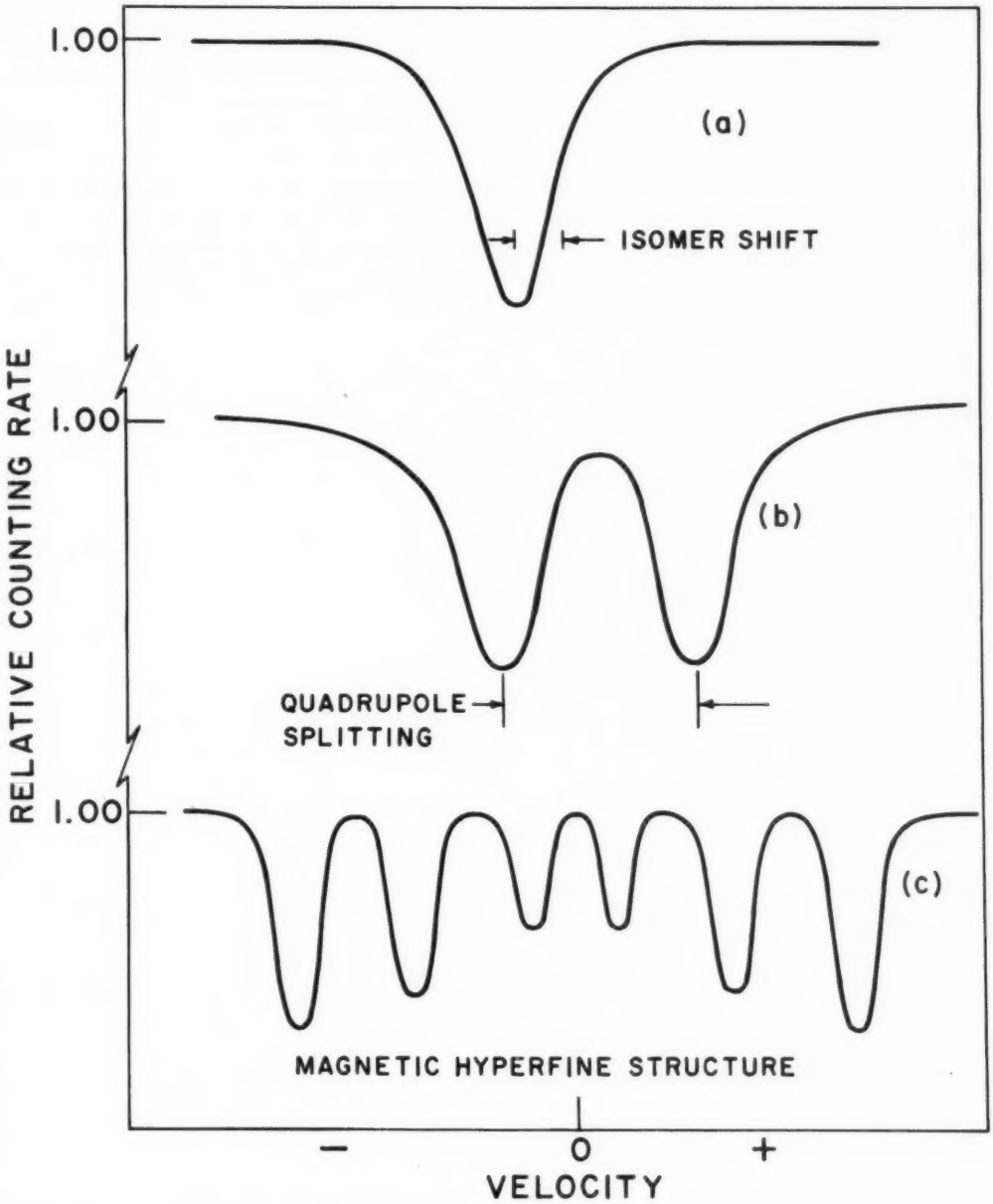

Figure 1. Idealized Mössbauer absorption spectra illustrating the appearance of: (a) an isomer shift, (b) a simple quadrupole interaction, and (c) a pure magnetic hyperfine interaction.

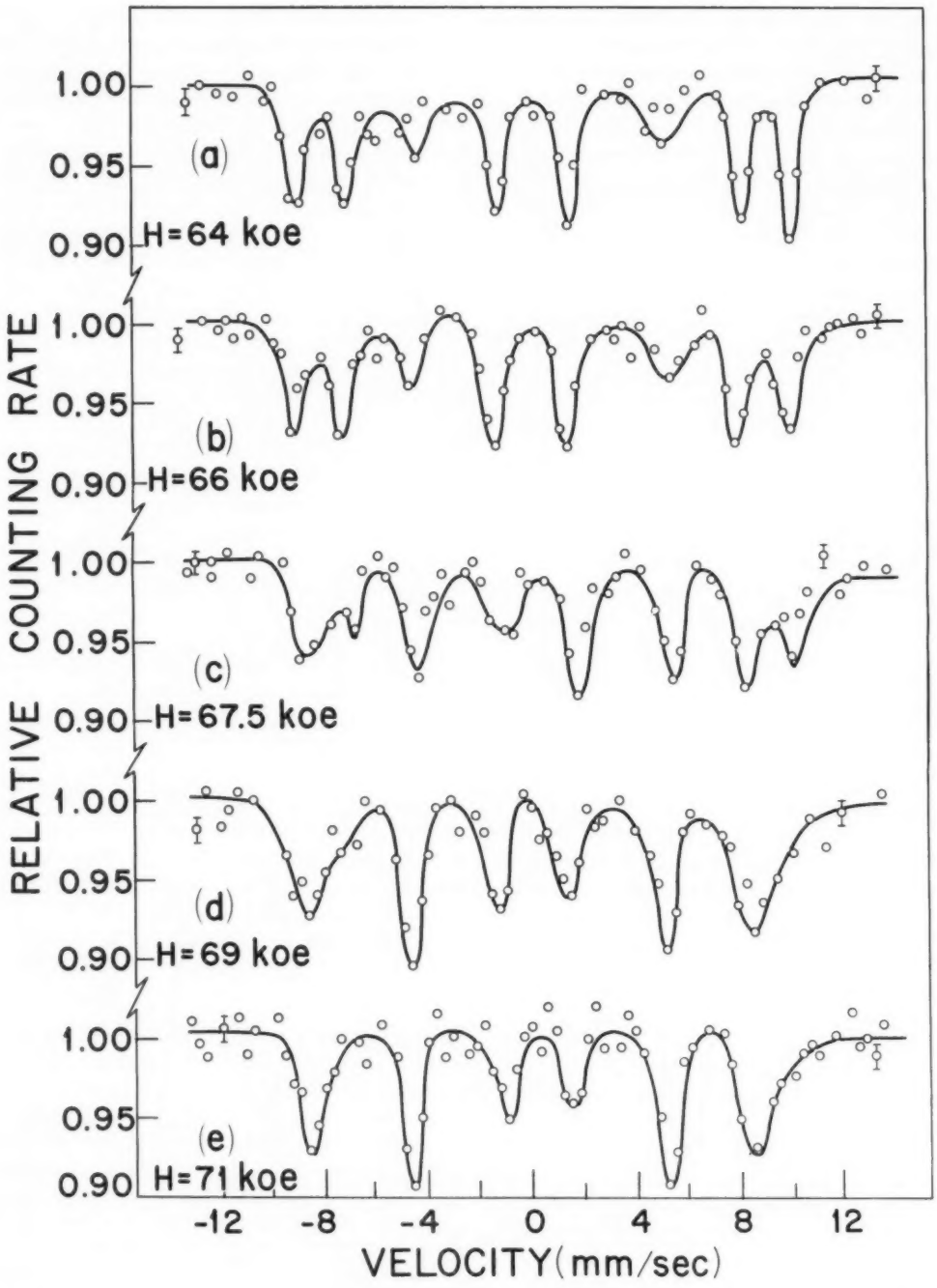

Figure 2. Absorption spectra using the same source and absorber as in Fig. 1, with an applied external magnetic field: T=80° K for all spectra; (a) H_0=64 kOe, (b) H_0=66 kOe, (c) H_0=67.5 kOe, (d) H_0=69 kOe, (e) H_0=71 kOe. The sequence shows the Mössbauer patterns in going through the spin-flop region.

as shown in Fig. 2(b). The 3:2:1:2:3 intensity ratios shown in Fig. 1(c) correspond to a random (isotropic) orientation of directions for H_n.

In materials which are not naturally magnetically ordered, the application of an external magnetic field produces a hyperfine spectrum by interacting directly with the Fe^{57} nucleus. In many substances of interest, the external magnetic field H_0 adds vectorially to an induced internal field (in the case of paramagnetic iron) or to the natural internal field in an ordered system. The magnitude and direction of the resultant hyperfine field H_n is measured in the Mössbauer experiments. At the National Magnet Laboratory at MIT, sponsored by AFOSR, Dr. Arthur J. Freeman, Associate Director, Dr. Norman Blum and Dr. Richard Frankel, Research Staff Members, and Prof. Lee Grodzins, of the MIT Physics Department, have been carrying on an extensive investigation of these magnetic properties of solids using the Mössbauer effect and magnetic fields up to 180 kilogauss.

The unique facilities for generating and using high magnetic fields at the National Magnet Laboratory have already been applied in an active program which has demonstrated the usefulness and importance of high fields for Mössbauer studies. External fields in combination with the Mössbauer effect allow

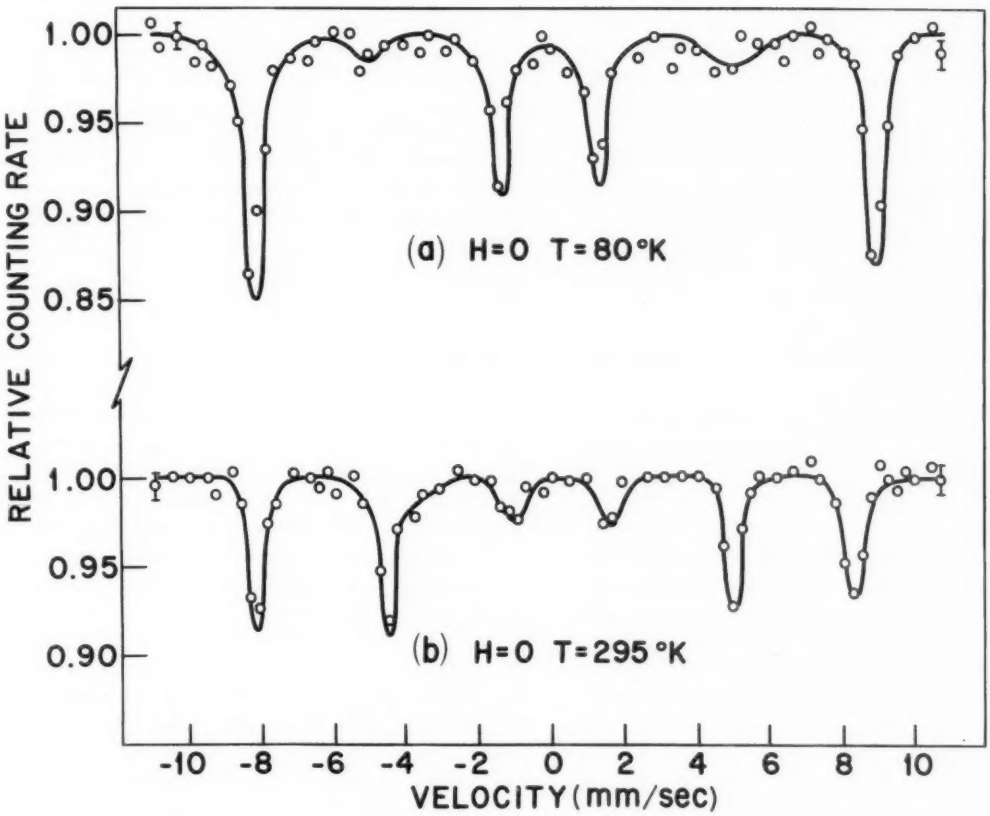

Figure 3. Mössbauer absorption spectra for an unsplit Co^{57} in Cu source vs. a single-crystal α-Fe_2O_3 sample oriented so that the gamma rays propagate along the crystallographic trigonal axis: (a) for $H_0=0$, $T=80°K$; (b) for $H_0=0$, $T=295°K$. This shows the effect on the Mössbauer pattern of going through the Morin transition ($T_M \approx 260°K$).

measurements to be made of the sign of the hyperfine field acting at the nucleus. It is now well known that it was found to be, quite surprisingly, negative in ferromagnetic metals using the Mössbauer effect. Furthermore, the high magnetic fields also simplify the analysis of experiments by eliminating lines from Mössbauer spectra when using longitudinal fields, or by changing the relative intensities of the lines when using transverse fields. Using external magnetic fields, a technique for determining the sign of the hyperfine field relative to that in metallic iron has been developed, and used to show that the fields at Fe^{57} nuclei in Cr and Cu at low temperatures are positive, that is, opposite in sign to that in metallic iron.

While external fields are useful in systems which are magnetically ordered in zero magnetic field, they are indispensable when one wishes to study systems such as paramagnetic metals, salts, and alloys; impurities; and hard superconductors. In these cases, the magnetic field produces a polarization of the electronic-spin distributions thereby producing an effective magnetic field at the nucleus which, in general, is larger than the applied field.

As a typical and fairly simple example of how external fields may be used to study magnetically ordered systems, we shall describe in some detail the results for one of the common oxides of iron. The magnetic properties of hematite (α-Fe_2O_3) have been studied extensively by various workers using a number of different techniques over a period of several decades. Hematite has a rhombohedral unit cell containing four iron atoms arranged with their magnetic moments in antiparallel pairs so that (as a first approximation) the unit cell has no net moment. Below the Morin transition $T_M \approx 260^\circ K$, the moments are, respectively, parallel and antiparallel to the crystallographic [111] direction. For $T > T_M$ the moments lie in the basal (111) plane; the moments of the paired atoms are not precisely antiparallel, but are slightly canted towards one another in the basal plane to produce a weak ferromagnetic moment (the Dzyaloshinsky moment). Also, it is well known that, for a sufficiently large external magnetic field H_c, the sublattice magnetizations will suddenly rotate from along the [111] direction into the (111) plane; this sudden rotation of the direction of the sublattice magnetization at the critical field is the spin-flop phenomenon.

An oriented single-crystal absorber was prepared from a large number of small single crystals cut from a sample of natural hematite. The small crystals were oriented by X-ray diffraction analysis, mounted to form a tightly packed mosaic 5/8 inch in diameter, and polished to a thickness of 0.005 inch; the crystallographic [111] direction is normal to the plane of the disk. The Mössbauer source was the unsplit line from Co^{57} in copper. Figure 3 shows the velocity spectra obtained in the absence of an applied magnetic field: (a) for $T = 80^\circ K$, and (b) for $T = 295^\circ K$. The splitting is due to the internal field H_{int}, which is 515 kOe for $T = 295^\circ K$ and 540 kOe for $T = 80^\circ K$. The second and fifth lines of the spectra are nearly absent in Fig. 3(a) and appear enhanced in Fig. 3(b). This result indicates that the internal fields (and therefore the sublattice magnetizations) are parallel (or antiparallel) to the [111] direction in Fig. 1(a), and perpendicular to the [111] direction in Fig. 1(b). This is the Mössbauer-effect demonstration of the Morin transition.

In Fig. 4, there are a series of spectra similar to those in Fig. 1, but with an external field H_o, along the [111] direction which varies from 64 kOe in Fig. 2(a) to 71 kOe in Fig. 2(e). The absorber temperature is $80^\circ K$, well below T_M. In Fig. 2(a), at 64 kOe, lines one and six are split into resolved doublets, with a separation between doublet components corresponding to $2H_o = 128$ kOe; this comes about as a result of half of the Fe atoms having an internal field parallel to H_o, and half having an internal field antiparallel to H_o. Lines 2 and 5 are missing, as is expected for H_n parallel to [111]; H_n is the total (net) hyperfine field. The inner pair of lines (3 and 4) are also doublets, but are unresolved because the splitting is of the same magnitude as the line width. In 2(e), at 71 kOe, the spectrum appears qualitatively similar to Fig. 1(b). Here there is a single $H_n = (H_{int}^2 + H_o^2)^{1/2}$ which is the vector sum of the perpendicular components, H_{int} and H_o; we

see from the enhancement of the middle lines that the internal fields H_{int} have rotated perpendicular to the [111] direction. The remaining spectra in Fig. 2, (b), (c), and (d), show how the transition takes place as a function of H_o; all the atoms do not undergo

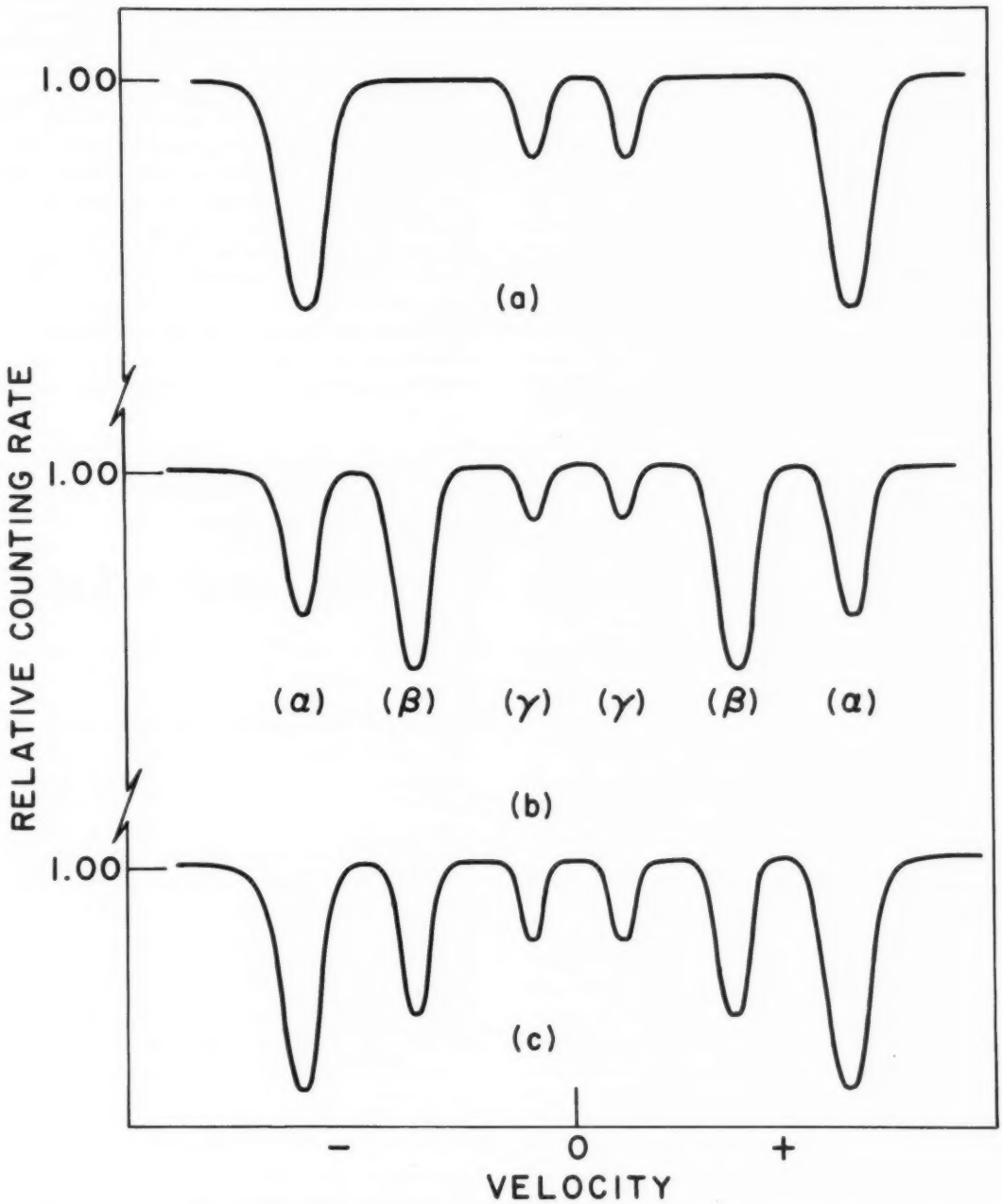

Figure 4. Relative intensities of the Mössbauer absorption lines for (a) H_n parallel to z, (b) H_n perpendicular to z, and (c) a random (isotropic) orientation of H_n with respect to the z-axis.

simultaneous rotation, primarily because of inhomogeneities in the alignment of the crystals making up the mosaic. This demonstrates the spin flopping, which for T = 80°K is seen to occur at $H_c = 67.5 \pm 3$ kOe.

The spin flop may also be inferred from the Mössbauer spectra obtained with a polycrystalline absorber. In this case, a sample consisting of commercial reagent grade α-Fe_2O_3 was bound into a Lucite matrix having a density of 1.0 mg/cm^2 Fe^{57}. The Mössbauer spectra at 80°K for different values of H_o are all qualitatively similar to Fig. 1(b), except that the outer lines are noticeably broadened. A plot of the width of the outer lines vs. H_o reveals a maximum in the vicinity of $H_c = 65$ kOe. A qualitative understanding of this behavior for a polycrystalline sample follows from the fact that the external field broadens the outer lines by contributing components displaced from the line center by as much as $H_{int} \pm H_o$ for those crystallites having their trigonal axes parallel to H_o. When $H_o = H_c$ the components contributing the most to the line broadening suddenly rotate by 90°, so that H_{int} is perpendicular to H_o; the contribution then appears centered at a velocity corresponding to $(H_{int}^2 + H_o^2)^{1/2}$, which is almost at the line center and contributes very little to the broadening. The middle is only slightly broadened because the parallel component, which contributes the most to the broadening, is forbidden by the selection rules governing the Mössbauer transition. Although not as dramatic as the single-crystal experiments, the Mössbauer experiments with a polycrystalline absorber also demonstrate that the spin flop in hematite occurs at about 65 kOe, for T = 80°K.

Similar techniques have been applied to $Y_3Fe_5O_{12}$ (yttrium iron garnet) which is a ferrite having two nonequivalent magnetic sublattices, to $KFe_{11}O_{17}$ (potassium ferrite) which is an "antiferrimagnet" having four nonequivalent magnetic sublattices, and to the magnetoelectric compounds $Ga_{2-x}Fe_xO_3$ and $Al_{2-x}Fe_xO_3$ which were shown by external-field Mössbauer experiments to be ferrimagnetic rather than canted antiferromagnets. These latter two materials exhibit a weak moment which is consistent with either a canted spin model or a nearly compensated ferrimagnetic model. The external-field Mössbauer experiments give unequivocal evidence that the latter model is correct.

The Mössbauer technique may be used together with external magnetic fields to elucidate the magnetic structure of matter. A simple illustration of the technique has been given. There are magnetic systems in which some of the rare earths play the dominant role, and some of these too may be studied by Mössbauer spectroscopy. The recent development and availability of intense-field large-bore magnets at the National Magnet Laboratory at MIT have made these experiments feasible. Research of this nature is essential to a detailed understanding of certain types of magnetic phenomena. ★

a step forward in ceramic storage-heater design

NORMAN E. SCAGGS, Fluid Dynamics Facilities Research Laboratory, ARL

The ceramic storage heater has been used for many years as a device for producing high-temperature gases with relatively small amounts of contamination. One of the more recent applications of the ceramic storage heater is a source of clean high-temperature air for use as a test medium in high-Mach-number ground-test facilities. Initially, the available ceramics were adequate in both materials and shapes. As the requirement for air at higher temperatures grew, problems began to appear in the satisfactory design of an appropriate heater. This article describes a solution to one of the major problems encountered in ceramic storage heaters.

The most critical region in a ceramic storage heater is the storage matrix, since it is exposed to the highest temperatures, suffers the most severe thermal shock, and is cycled through the largest temperature

ranges. Consequently, both the material and the shape of the storage matrix are very important. Originally, the storage matrix in most ceramic heaters was assembled from spheres, partly because this shape was available and partly because the sphere is an easy shape to manufacture. The storage matrix is also very easy to assemble when spheres are used. The spheres were quite satisfactory until the ceramics were heated to the softening temperature of the material. At this point, the high stress on the spheres caused them to fuse together to form a solid mass of ceramic, thus preventing air passage and, of course, making the heater unsatisfactory.

Due to the small area of contact between two spheres, the slightest load produces a very high stress at the point of contact. In a ceramic storage heater, the load is generated by the weight of the ceramics above each level in the matrix. The maximum bulk stress in most storage heaters is approximately 20 psi; but, at the point of contact between each sphere, this stress is several orders of magnitude higher. An obvious solution to this problem is to utilize a shape that provides a larger contact area. This is easier said than done because the shape must allow air to pass through it freely, must not fail from thermal shock, and must have the capacity for storing a sufficient amount of energy. The shape should also be easily manufactured and easily assembled.

The shape that emerged from all these considerations was a cored brick configuration as shown in Figure 1. The dimensions and material of the brick were determined by the specific requirements of the Aerospace Research Laboratories' heater. In the case of the facility at the Aerospace Research Laboratories, an air temperature up to $4{,}000^{\circ}R$ for a duration of 300 seconds at a mass-flow rate of 1 pound mass per second was specified.

The requirement for air at $4{,}000^{\circ}R$ limits the choice of materials for the top portion of the heater matrix to two materials; magnesium oxide or zirconium oxide. Since magnesium oxide slowly vaporizes in this temperature range, zirconium oxide was selected.

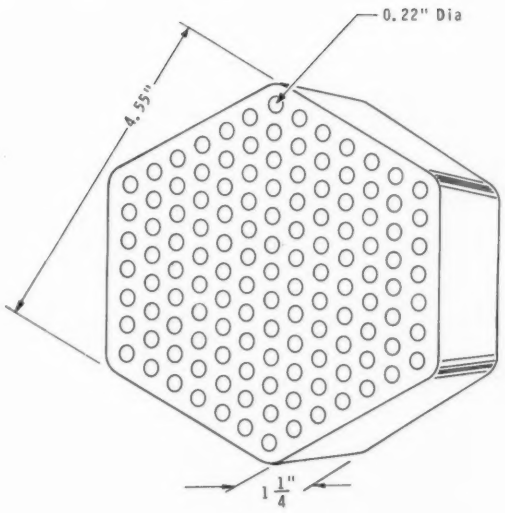

Figure 1. Cored brick configuration.

The lower portion of the heater is subjected to lower temperatures and, therefore, a wider variation of materials can be considered for application in this region. However, experience has shown that aluminum oxide is the most efficient material to use in this portion of the heater matrix. The material chosen must also be very dense to facilitate a large amount of energy storage and to permit high mass-flow rates. The weight of the ceramics counteracts the drag of the air flow. The densities of the zirconium oxide and the aluminum oxide in the ARL heater are 343 lbm/ft^3 and 241 lbm/ft^3, respectively.

The over-all size of the brick was determined by the thermal-shock characteristics of the material and the manufacturer's size capability. The hole diameter and the number of holes were determined by balancing the thermal-shock characteristics against the energy-storage capacity of the material. Both the hole diameter and the number of holes influence the resistance to air passage and these factors, coupled with the density of the bricks, fix the maximum allowable mass flow through the heater before the bricks start to float. The bricks will start to float when the drag is equal to the weight of the bricks.

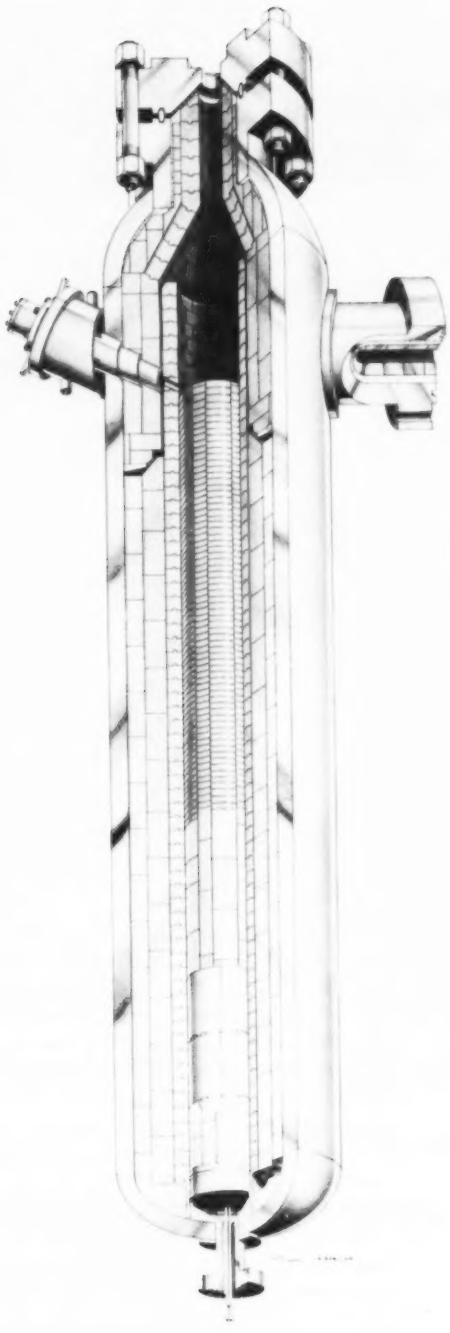

Figure 2. Cored brick storage heater.

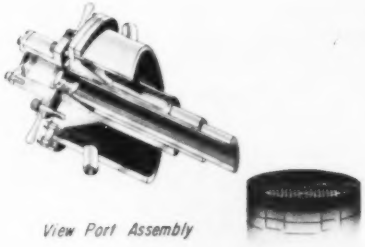

View Port Assembly

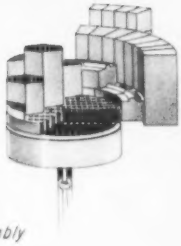

Grating and
Insulation Assembly

The present configuration of the cored brick storage heater at the Aerospace Research Laboratories is shown in Figure 2. The top seven and one half feet of the storage matrix are made of zirconium-oxide cored brick. The construction of the storage matrix starts at the very bottom, and the holes in each successive layer of bricks are aligned so that finally the matrix is a cylinder of ceramic twelve and one half feet long with air-passage holes through it.

The operation of the heater consists of blowing combustion gases from a methane-air-oxygen burner, which is installed at the top of the heater, down through the storage matrix where the energy is absorbed. When the desired amount of energy is stored, the burner is shut off and clean, dry air is blown through the heater from bottom to top, retrieving the energy as it progresses through the heater. In this manner, the air will reach approximately the temperature of the top portion of the matrix. The maximum allowable temperature profile in the ARL heater is shown in Figure 3. With this profile, an air temperature of 4,000°R can be achieved.

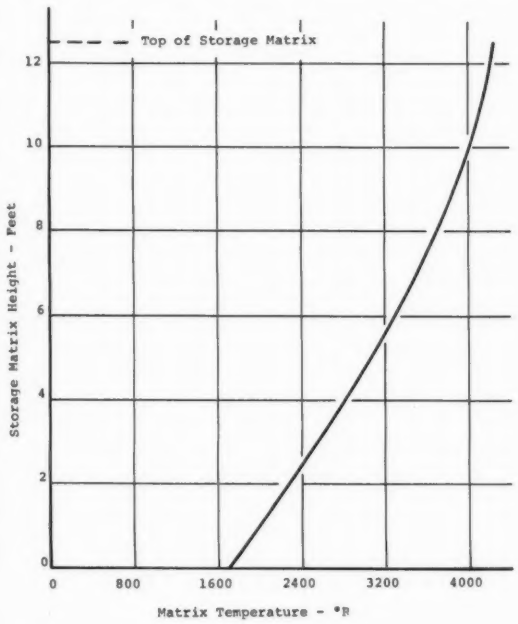

Figure 3.
Maximum allowable matrix temperature profile.

A specific example of an actual test on the ARL heater is shown in Figures 4 and 5. The heater temperature profiles before and after the test are shown in Figure 4. Figure 5 shows the variation in the air temperature produced during the test. The variation in air temperature during this test was 40°R at a mass-flow rate of 0.75 lbm/sec over a time duration of 250 seconds.

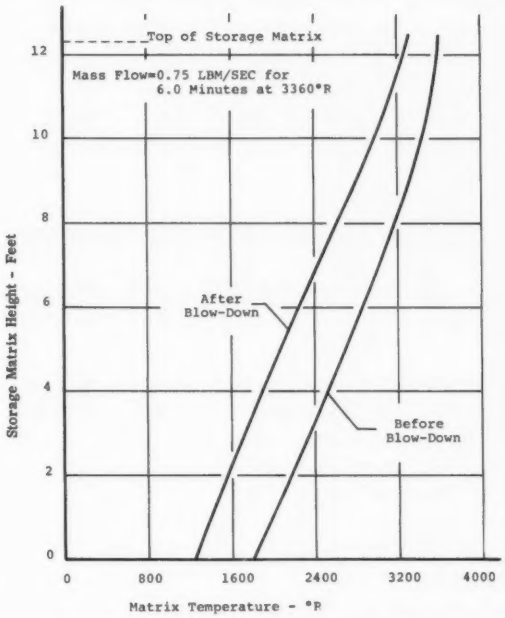

Figure 4. Example of heater performance.

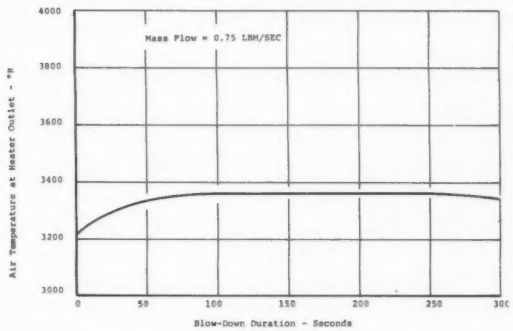

Figure 5. Example of heater performance.

The advantages of the cored brick configuration over spheres for the storage matrix can be summarized as follows:

1. The elimination of high stresses per-

mits a higher maximum temperature profile for a particular ceramic material since the ceramics can be heated nearer their melting points without fusing.

2. A bonus effect results when cored brick is used instead of spheres, since the drag on the cored brick is only one half the drag on spheres for a given mass-flow rate. The low resistance to air flow reduces the percentage of flow through the insulation surrounding the storage matrix, thus resulting in a final air temperature nearer the top brick temperature.

3. Both 1 and 2 above contribute to a higher maximum air temperature producable in a storage heater.

4. The lower resistance to air flow also permits higher mass-flow rates through the storage matrix before flotation of the bricks occurs.

The cored brick storage heater at the Aerospace Research Laboratories is the first of its kind at an Air Force installation. The performance of the heater during the short time it has been in operation is very encouraging. Further evaluation of this particular configuration continues as the heater is utilized to provide air at temperatures between 3,000°R and 4,000°R for a ground-test facility. ★

turbulent heat transfer in an insulated pipe

J. W. GORESH, Fluid Dynamics Facilities Research Laboratory, ARL

The general problem of turbulent forced-convection heat transfer in cylindrical pipes is of considerable practical interest. In many cases where high-temperature gases flow subsonically through insulated pipes, the engineer is often required to design tubes which produce uniform exit-temperature profiles. This study, which considers the case where the wall-heat flux is zero, provides a method of finding the minimum-length mixing tube. Tubes having any wall-heat losses will have greater mixing lengths.

The fluid enters the pipe with a nonuniform temperature and a fully developed turbulent velocity profile. At succeeding axial stations, due to the radial conduction and turbulent mixing, the temperature profile will deviate from the entering profile until a uniform profile is approximately achieved.

The analysis is similar in the general mathematical approach to that presented by Latzko (1) and Fettis (2) for an isothermal wall. They also assumed a one-seventh power velocity profile, a simplified eddy diffusivity, and a Prandtl number of unity.

Results for selected entrance conditions are presented which show the adjustment of the temperature profile down the pipe. A schematic diagram showing the coordinate system is given in Figure 1.

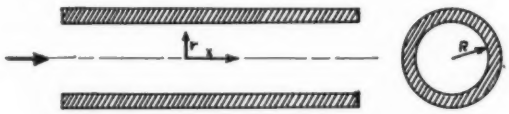

Figure 1. Diagram of co-ordinate system.

We have considered the section of pipe to the right of x=0, where the wall-heat flux is equal to zero. The flow possesses a fully developed turbulent velocity profile and a selected entrance-temperature profile at x=0.

Subject to the limitations given below, the steady-state energy equation is:

$$\rho\, C_p\, u \frac{\delta \theta}{\delta x} = \frac{1}{r} \frac{\delta}{\delta r} (r q_r), \qquad (1)$$

where x = the axial distance of a point of the fluid from the inlet,
r = the radial distance of that point from the center line.
θ = the temperature excess of a point over surface temperature,
ρ = the density of the fluid,

C_p = the specific heat at constant pressure,

u = the velocity of the fluid and

q_r = the radial heat flux.

In writing the energy equation (1), the usual basic assumptions are adopted:

a. The fluid properties are assumed constant.

b. Viscous dissipation is negligible.

c. Axial diffusion of heat is negligible compared to the axial convection.

d. It is also assumed that the flow is hydrodynamically fully developed.

The statement of the problem is completed when the boundary conditions are specified for the function $\theta(r,x)$. At the inner surface of the pipe we have:

$$k_w \left.\frac{\delta \theta (r,x)}{\delta r}\right|_{r=R} = q_w = 0, \quad (2a)$$

where k_w and q_w represent the gas conductivity and flux at the wall.

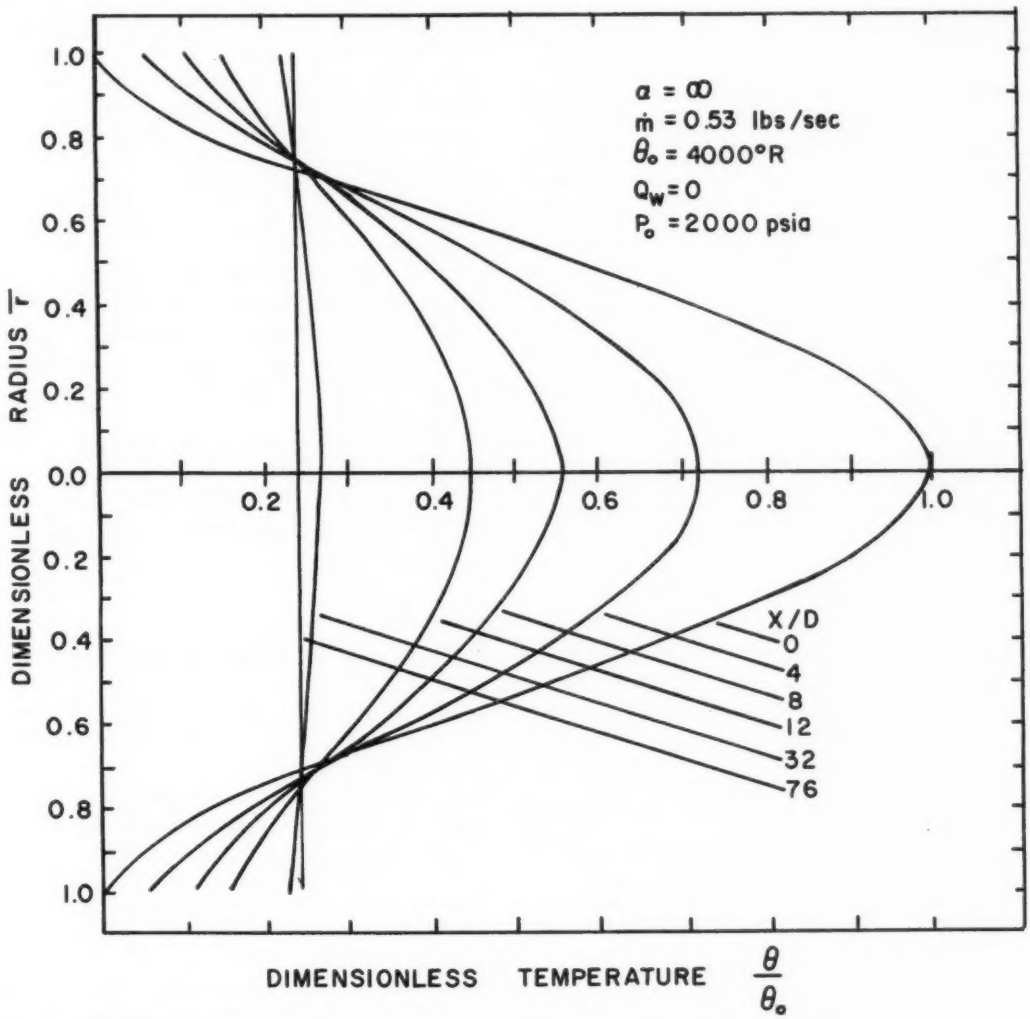

Figure 2. Radial temperature profiles at different axial distances.

The fluid temperature, at the entrance (i.e., x = 0) is given by the following:

$$\theta\ (r,0) = \theta_0\ f(r). \qquad (2b)$$

The equations (1), (2a), (2b), and the imposed condition that no infinite temperatures exist, constitute the mathematical statement of the problem.

The method used in obtaining a solution to equation (1) for the specified boundary conditions was analogous to that first used by Fettis (2) in solving the isothermal problem with a uniform entrance-temperature profile. However, to obtain a nontrivial solution to the present case, it was necessary to assume that the fluid entering the pipe had a nonuniform temperature profile. The eigenvalues and eigenfunctions remain unchanged for any entrance-temperature profile because neither depends on the initial temperature distribution. In the chosen numerical example, the initial temperature distribution was represented by the following:

$$\theta\ (\bar{r},0) = \theta_0\ f(\bar{r}) = \theta_0\ (1-\bar{r}^2)^2,$$

where θ_0 is the initial center-line temperature and the nondimensional radius $\bar{r}$ is the ratio of the radial variable r to pipe radius R.

The adjustment of the temperature from radial variation to a uniform distribution at succeeding axial stations is shown in Figure 2.

The engineer is often required to design mixing tubes with varying degrees of wall-heat losses. Thus, these calculations provide him with the length of a perfectly insulated tube for turbulent flow. This is the minimum-length mixing tube, since any wall losses will require a greater length. Calculations for imperfectly insulated pipes were presented in reference (3). ★

REFERENCES

(1) *Latzko, H., NACA TM 1068, 1944, (original in German).*

(2) *Fettis, H. E., "On the Eigenvalues of Latzko's Differential Equation," ZAMM, Vol. 37, Nos. 9 and 10, September/October, 1957.*

(3) *Goresh, J. W., "Heat Transfer in Cylindrical Pipes with Fully Established Turbulent Flow and Exposed to a Uniform Temperature Environment," Journal of Heat Transfer, Paper No. 65-WA/HT-16.*

recent AFCRL rocket firings

Cosmic-Ray Measurements: An Aerobee-150 sounding rocket was launched by AFCRL from Fort Churchill, Canada, on August 8 to study cosmic-ray nuclei as a function of solar activity. The experiment was designed to learn more about the sun's contributions to the flux of high-energy particles reaching the earth. The rocket carried a 240-pound payload to an altitude of 196 km. Approximately 90 seconds after launch, 4 doors on the nose cone opened to expose photographic emulsion plates to cosmic radiation. The nose cone was subsequently recovered by parachute. Specific objectives of the test were:

1) To study primary cosmic-ray nuclei at the very lowest energy during a period of low sunspot number.

2) To compare relative numbers of low-energy cosmic-ray nuclei of different atomic numbers with cosmic-ray abundance.

3) To determine if significant numbers of heavy nuclei are emitted by the sun during quiet times.

4) To measure the primary flux of low-energy protons and alpha particles.

Robert C. Filz is the project scientist for this experiment. (Space Physics and Aerospace Instrumentation Laboratories)

Daytime Aurora: AFCRL launched an Aerobee-150 sounding rocket from Fort Churchill, Canada, on August 11 to study the upper atmosphere during a daytime auroral event. The Aerobee carried a 225-pound payload to an altitude of 210 km. Instrumentation included a 1-meter Ebert instrument with a photomultiplier-tube detector to measure the line-emission spectra of the upper atmosphere above 80 km. Purpose of the experiment was to confirm theoretical estimates of the intensity for several emission lines. The nose cone was retrieved by parachute. Project scientist for the experiment is Dr. Sam Silverman. (Upper Atmosphere Physics Laboratory) ★

ELECTRONICS DIVISION
AFOSR

light-scattering homodyne spectroscopy

In the development of a theory of liquid behavior, a crucial test of propositions occurs at and near critical temperatures. These are temperatures, for given conditions of pressure and specific volume, where (often dramatic) state changes take place--for example, when water changes to ice or when liquid helium becomes superfluid. In pursuit of experimental ways to evaluate existing mathematical models for fluids, research personnel of the Columbia Radiation Laboratory (CRL), supported under the Joint Services Electronics Program have, for the first time, observed and measured the frequency spectra of time-dependent concentration fluctuations in liquids close to the critical temperature.

These results were made possible by the use of a special spectrometer, the laser homodyne spectrometer, designed and built by the CRL staff in 1963. The spectrometer functions with light in much the same way that a Doppler radar functions with microwaves. In the present form of the apparatus (see Figure 1), the output of a helium-neon laser of wave length 6328Å is divided by a

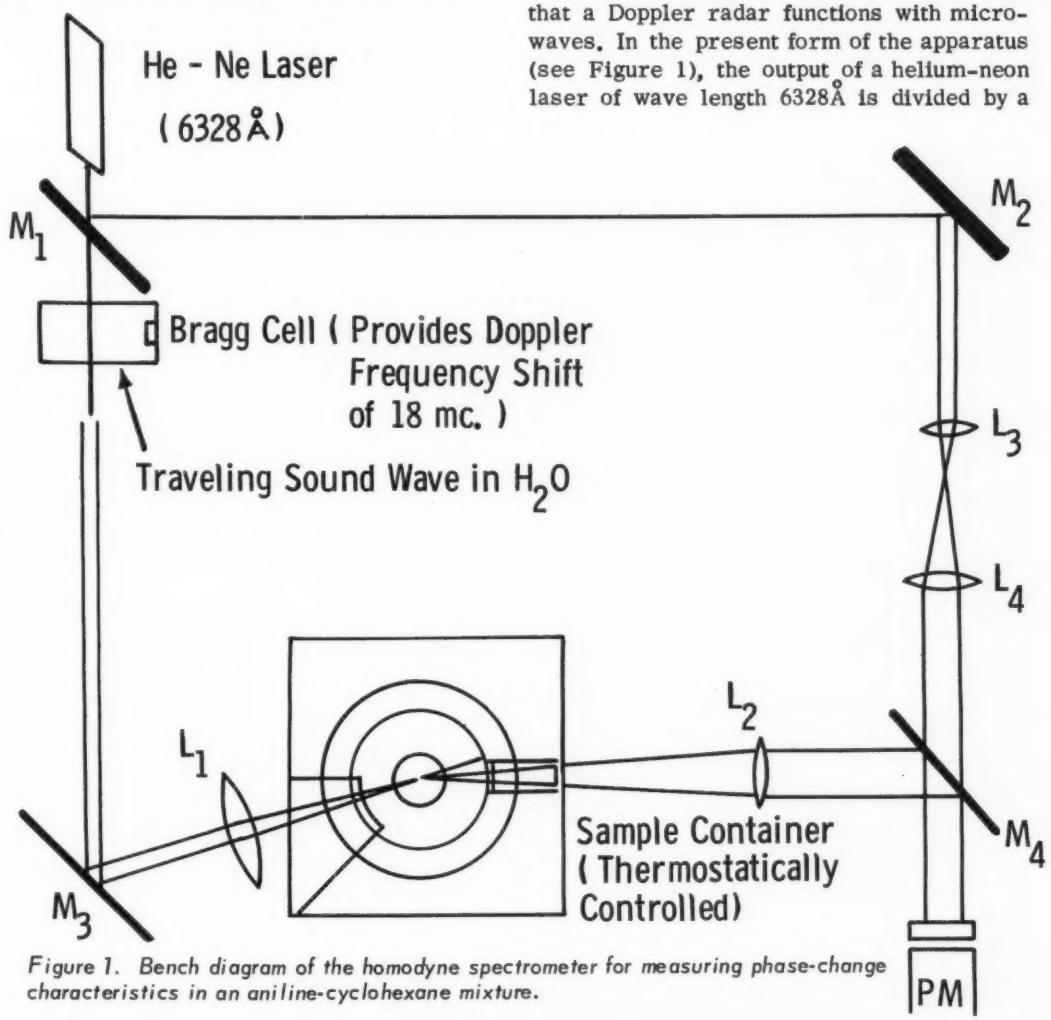

Figure 1. Bench diagram of the homodyne spectrometer for measuring phase-change characteristics in an aniline-cyclohexane mixture.

semireflecting mirror (M_1). The major beam is given a small frequency offset of 18 Mc/sec by reflection from traveling sound waves in water, and is then transmitted through the sample under study via mirror M_3. Light scattered in a particular direction by the sample is then recombined with the minor beam (at mirror M_4), which plays the part of the local oscillator in the analogous microwave system. The recombined beams form the input to a photomultiplier. Since the interference between the two beams is modulated at the offset frequency, only that part of the output from the photomultiplier which lies in a narrow band of frequencies around 18 Mc/sec is amplified and processed by the spectrometer. In effect, the spectrometer measures the coefficients in a plane-wave expansion for the scattered field. A conventional spectrometer would measure intensity.

Light scattered from a liquid (Rayleigh or Tyndall scattering) is usually considered to have a spectral distribution identical with the exciting radiation. The reason for this is that the resolution required to observe the line shape in such a case is about 10^{13}, which exceeds that provided by any classical spectrometer. This high resolution, however, is easily attained with a laser source and homodyne spectrometer. A successful demonstration of this was achieved by resolving the spectrum of light scattered from a cyclohexane-aniline mixture in a constant-temperature enclosure. The scattered light was observed to have a Lorentzian line shape of width proportional to the difference between the sample temperature and the critical temperature for the mixture. In addition, the line width was shown to be proportional to $\sin^2(\theta/2)$, where θ is the scattering angle. All of these observations are in qualitative agreement with the theory first formulated by Landau and Placzek.

Of perhaps more fundamental interest are similar measurements on single-component systems. The width of the Rayleigh line provides a measure of a relaxation time τ which characterizes the time scale on which spontaneous density or concentration fluctuations appear and disappear in the medium. This parameter τ now accessible to measurement may, in turn, be related to thermodynamic properties evaluated in the neighborhood of the critical point. In this region some quantities--e.g., specific heat--are strongly varying and poorly measured by conventional methods. By means of statistical mechanical theory, thermodynamic quantities can be related to molecular forces. New accurate data through the critical region are expected to provide a sensitive test for present and future statistical models for the liquid state. Studies in one-component monatomic liquids will provide the most tractable case for comparison with theory.

Preliminary results on light scattered by pure carbon dioxide have been obtained. The program for the immediate future includes a refinement of these measurements and extension to the noble gases, xenon and argon.

Understanding the behavior and properties of fluids is of particular interest to the Air Force, not only because our aircraft must operate in the fluid of the atmosphere, but also because the flow characteristics and properties of fuels, combustion products, coolants, etc., must be understood to advance the state-of-the-art of propulsion-system design, and because weather forecasting is so dependent upon understanding the phase changes of water.

The homodyne spectrometer measurements were made and reported by Drs. S. S. Alpert, Y. Yeh, and E. Lipworth, members of the Columbia Radiation Laboratory, which is directed by Professor Robert Novick. ★

REFERENCES

(1) Joint Services Electronics Program, Contract No. DA 28-043 AMC-00099(E).

(2) Alpert, S. S., Y. Yeh and E. Lipworth, "Observation of Time-Dependent Concentration Fluctuations in a Binary Mixture Near the Critical Temperature, Using a He-Ne Laser," Phys. Rev. Letters, Vol. 14, 486, 1965.

DATA SCIENCES LABORATORY, AFCRL

DOG SILHOUETTES AND OTHER ARBITRARY SHAPES BY COMPUTER

A crude stick figure of a dog (Figure 1), traced on a computer cathode-ray tube (CRT) output-input scope with a light pen, expands and takes shape on the tube face to become a full silhouette of a German shepherd. An "X" traced on the tube is transformed into a square, a single dot into a circle, and a series of apparently random lines of various lengths and curvatures becomes a meaningful arrangement of several objects.

These transformations (actually inverse transformations because, in this case, the computer had previously derived the simpler geometrics from the more complex shapes) are being studied to define the capabilities of a unique pattern-recognition technique. Although the concept has been under mathe-

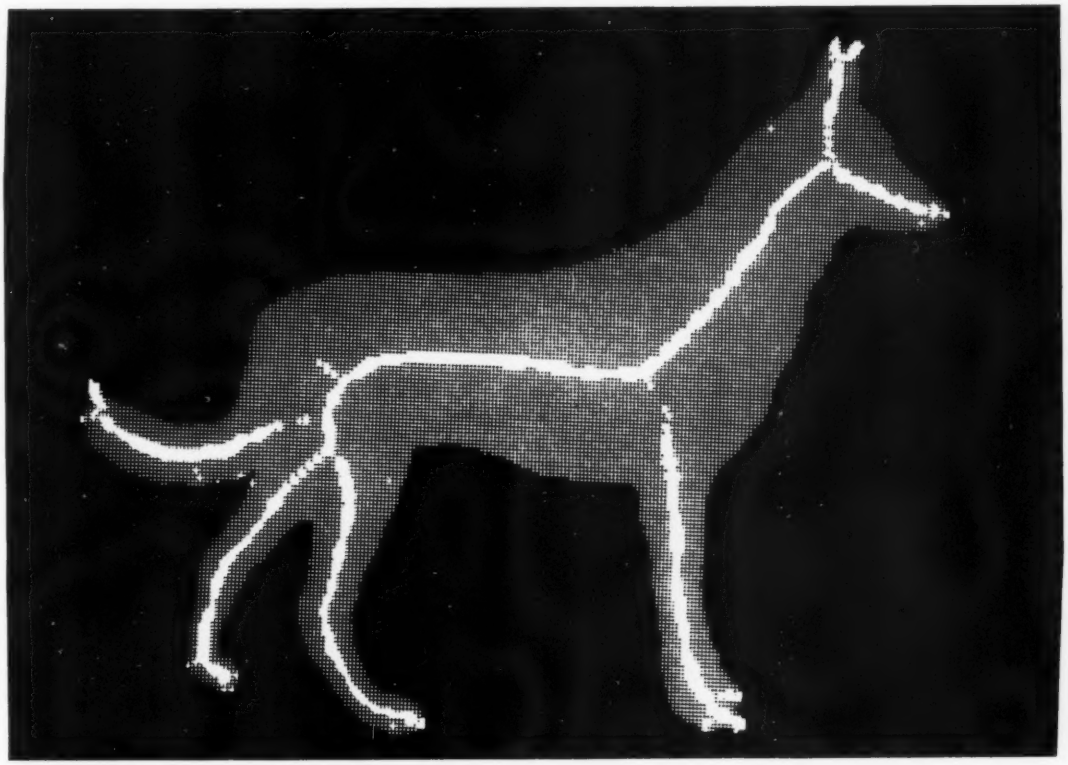

Figure 1. Shape of a German shepherd as reproduced by cathode-ray-tube computer output on a 256 x 256–element grid. The shape was reconstructed from the transformation pattern represented by the white medial axes.

matical investigation for several years by Harry Blum of AFCRL, it has only been within recent months that a computer program has been formulated for making actual pattern transformations. The computer simulation program for analyzing the pattern-recognition technique has been developed and carried out by Otis Philbrick, also of AFCRL. The computer being used is a small general-purpose digital computer (Digital Equipment Corporation PDP-1). The CRT images are presented on a grid of 256 by 256 elements.

A basic advantage of this pattern-recognition technique, known as Medial Axis Transformation, is that it permits the recognition of patterns of arbitrary shapes; it does not have the geometrical constraints associated with other pattern-recognition methods. (The best examples of extremely rigid geometrical constraints are found in automatic-recognition schemes requiring the stylized numbers and letters we see on our credit cards and bank checks.)

Just how transformations from a complex shape to simple descriptive lines are made is best illustrated by Blum's grass-fire analogy. The grass fire begins at the edge of the pattern and spreads with a uniform velocity into the pattern. Suppose the pattern edge--where the grass fire originates--is a square. At each corner of the square, the fires on the two nearest sides intersect. As the grass fire burns inward, the two fronts continue to meet. Where they meet is the medial axis. For a square, the two intersecting fronts trace a diagonal line inward toward the center of the square. Ultimately, the four lines originating at each of the four corners of the square come together at the center. The result is a well-defined "X" that has been drawn in time.

The "X" is the transformation pattern of the square. The stick figure of the German shepherd, noted earlier, and the aircraft shape (Figure 2) were similarly derived. Knowledge of the time sequence of the formation of the residual line, or the medial axis, is fundamental to the technique. Acting upon this knowledge, the computer can take the simple derived lines and perform the reverse transform to reconstruct the original object. By way of further example, we see from the above description that a single line represents a transformed V. But without knowledge of the time-rate at which the line was drawn, there is no way to determine whether the V had an angle of 30 degrees, 130 degrees, or any value between.

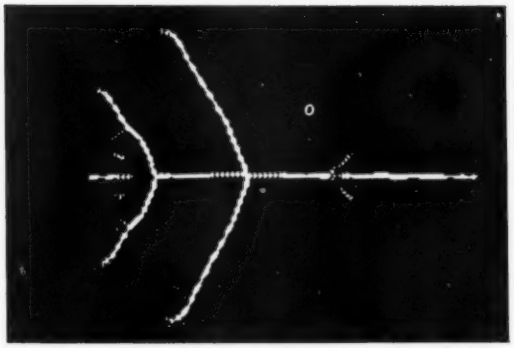

Figure 2. Aircraft shape reconstructed in the same manner as Figure 1. Both figures represent progress toward the reduction of complex shapes to simpler ones which a computer can analyze and process automatically.

Computer simulation of the technique does not mean that the technique is approaching operational feasibility. But the simulation studies have shown Blum and Philbrick the potential of the system, and are helping to define parameters for an ultimate operational system.

Automatic pattern-recognition systems are increasingly needed to process the mushrooming growth of pictorial data that must now be examined by laborious manual methods. Two prime examples are reconnaissance photographs and the huge volume of cloud photographs transmitted daily to earth by weather satellites. But another important potential application is the transmission of visual data over narrow-band channels. It takes more band width and power to transmit complex visual patterns than to transmit simple ones. By transmitting only the transformed patterns, using the Medial Axis Transformation technique for later inverse transformation at the receiving terminal, the technique may provide means for conserving band width and power. ★

PROFILES

Messrs. Otis Philbrick (left) and Harry Blum (right), of the Data Sciences Laboratory, AFCRL, are developing a unique pattern-recognition technique described in "Dog Silhouettes and Other Arbitrary Shapes by Computer," appearing in this issue of the Review. Mr. Philbrick, an electronics engineer, received his B.S. from M. I. T. in 1964 and his M.S. from Northeastern University in 1966. He began working for AFCRL while a University Co-op student, in 1962. Recently, he has been designing, developing, and operating special-purpose computer programming systems to simulate and test mathematical models of picture-analysis and transmission systems. Mr. Blum, a physical scientist, received his B.E.E. from Cornell University in 1949, and his M.E.E. from Syracuse University in 1958. From 1958 to 1960, while assigned to the SHAPE Air Defense Technical Center in The Hague, Netherlands, he built and headed a group to handle problems of ballistic-missile warning and defense. Since 1960, he has been doing research at AFCRL on a new class of machines for dealing with shape and perception that depend on propagative processes for the interaction and organization of information.

Major John P. Thomas, an aerospace research engineer in the ARL Hypersonic Research Laboratory since August 1963, has been studying heat transfer at the base of fins on hypersonic model configurations. He discusses "The Effect of Aerodynamic Control Surfaces on High-Speed Vehicles" in this issue of the Review. Major Thomas was graduated from the University of Colorado in 1949 with a B.S. in Aeronautical Engineering and a B.S. in Mechanical Engineering. He also has an M.S. in Mechanical Engineering (1957) from Purdue University, where he specialized in propulsion, and a Ph.D. in Aeronautical and Astronautical Engineering from The Ohio State University (June 1966). Major Thomas entered the Air Force in January 1951 and completed his Aviation Cadet training with a "distinguished" rating. Commissioned in 1952 in the regular Air Force, he flew B-29's and B-47's, and was an instructor on the B-47 flight simulator. He is a member of several professional societies.

Mr. Norman E. Scaggs has been with the Fluid Dynamics Facilities Research Laboratory, ARL, since August 1963, as Project Engineer on the ARL 30-inch hypersonic wind tunnel. He is responsible for the operation of the facility, and acts as consultant for all aerodynamic tests performed in it. Before joining ARL, Mr. Scaggs was employed as a research associate at The Ohio State University. While there, he completed almost 60 hours of courses toward the master's degree in Aeronautical and Astronautical Engineering. Previously, he had received the Bachelor of Aeronautical Engineering degree from Ohio State, in 1957, and served in the Air Force for three years, from 1957 to 1960, as an Aircraft Maintenance Officer. His article, "A Step Forward in Ceramic Storage-Heater Design," appears in this issue of the Review.

Mr. John W. Goresh, whose article, "Turbulent Heat Transfer in an Insulated Pipe," appears in this issue of the Review, is currently assigned to the Fluid Dynamics Facilities Research Laboratory at ARL. His present research interests include (1) turbulent heat transfer due to hot gases flowing through small-diameter cylinders; (2) dissociation of gases at high temperatures and pressures; and (3) reduction of model data at hypersonic speeds. From June 1960 to November 1962, before coming to ARL, Mr. Goresh was at the Dyna Soar Systems Project Office. As Project Engineer under the Dynamics Section, he was responsible for the aeroelastic and dynamic-load design problems encountered in designing the Dyna Soar vehicle. Mr. Goresh has a B.S. in Mathematics from Eastern College, Quincy, Mass. His graduate studies have included mathematics, physics and aeronautical engineering at Boston University, Northeastern University, and Ohio State University, respectively.